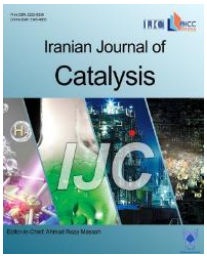

Iran. J. Catal. 2026; 16(1): 38-49

Iranian Journal of Catalysis (IJC)

https://doi.org/10.57647/ijc.2026.1601.03

Research Article

Evaluation of Fe-Cu Catalysts Supported on Magnesium Oxide in Methane Combustion Reaction

Abdullah Irankhah[1,*], Zahra Hossein Mirzaei[1], Atieh Ranjbar[2]

[1] *Hydrogen and Fuel Cell Research Laboratory, Department of Chemical Engineering, Faculty of Engineering, University of Kashan, Kashan, Iran*

[2] *Department of Chemical Engineering, Tafresh University, Tafresh 39518 79611, Iran*

[*] **Corresponding authors:** irankhah@kashanu.ac.ir

Article History:

Received:
9 June 2025

Revised:
25 September 2025

Accepted:
24 October 2025

Published Online:
25 November 2025

Published in Issue:
31 March 2026

Abstract

The catalytic performance of xFe/MgO (x=10, 15, 20 wt.%) and Cu-promoted 15Fe-yCu/MgO (y=3, 5 wt.%) catalysts, fabricated via impregnation techniques on a precipitation-derived MgO support, was investigated for methane combustion. Maximum activity was observed for the 20Fe/MgO formulation, exhibiting light-off temperatures T_{10} and T_{50} of 412°C and 463°C, respectively. This superior activity is correlated with its physicochemical properties, namely a high specific surface area (49.70 $m^2 \cdot g^{-1}$), small crystallite size (22 nm), and presence of abundant Fe active sites on the surface of MgO or within $Mg_{1-x}Fe_xO$ solid solution. In contrast, Cu promotion detrimentally affected performance, an effect ascribed to the blockage or fundamental alteration of the active sites and agglomeration of particles. The 20Fe/MgO catalyst further demonstrated notable operational stability, maintaining >80% CH_4 conversion during a 25-hour time-on-stream analysis at 550°C. XRD characterization of the spent catalyst indicated progression of solid solution formation following the reaction.

Keywords: Fe-Cu catalysts; Methane combustion; MgO; Precipitation; Solid solution

Cite this article: A. Irankhah, Z. Hossein Mirzaei, A. Ranjbar, Iran. J. Catal. **16** (2026) 38-49. https://doi.org/10.57647/ijc.2026.1601.03

1. Introduction

CH_4, the primary component of natural gas, is a potent greenhouse gas [1,2]. Despite its environmental impact, methane remains a crucial energy source considering its high energy density and abundance. Traditional methane or flame-based oxidation operates at high temperatures (typically above 1500°C) and often leads to the formation of nitrogen oxides (NO_x), carbon monoxide (CO), and unburned hydrocarbons (UHCs). These emissions contribute to air pollution, acid rain, and climate change, thereby demanding cleaner and more efficient combustion technologies [3,4]. Through the use of heterogeneous catalysts (catalytic combustion of methane, CMC), complete oxidation of methane occurs at significantly lower temperatures (typically 300–800°C). As CMC enhances fuel efficiency, reduces energy losses, and mitigates the formation of harmful pollutants, it is utilized in gas turbines, residential heating systems, and automotive exhaust treatment, where emission control and energy efficiency are critical. In catalytic methane combustion, methane and oxygen are adsorbed and react to form CO_2 and H_2O. The efficiency of catalytic combustion depends on the catalyst's ability to activate methane at low temperatures while maintaining stability under high-temperature operating conditions [5, 6]. Commonly studied catalysts for methane combustion include noble metals or metal oxide catalysts. Palladium

(Pd) [7] and platinum (Pt) [8] are the most active noble metals for methane oxidation, with Pd-based catalysts generally exhibiting superior performance at lower temperatures. These metals are typically supported on high-surface-area oxides such as alumina (Al_2O_3) [9], ceria (CeO_2) [10], or zirconia (ZrO_2) [11] to enhance dispersion and thermal stability. In addition to the high cost of noble metals, these metals also suffer from deactivation due to sintering, poisoning, or phase changes (e.g., PdO ↔ Pd transitions), especially at higher temperatures [12]. To develop more economical alternatives, the researchers have explored (transition) metal oxides, including CuO [13], Co_3O_4 [14], Fe_2O_3 [15], MnO_x, CeO_2 [16,17], perovskites like $LaMnO_3$[18], $LaCoO_3$ [19], $BaMnAl_{11}O_{19}$ hexaaluminates [20] and Mn_3O_4 [21], $CoAl_2O_4$ [22] spinels. Thoughthe activity of metal oxides is lower than that of noble metals, these materials possess good thermal stability and resistance to poisoning. To improve the performance of the metal oxides, they are usually doped or structurally engineered to gain special nanostructures.

Among the metal oxides used, MgO, with its high melting point and surface area, basic properties, and abundant availability, has been widely studied as a support or promoter in catalytic processes. A CoMgO solid solution prepared by the combustion technique was studied by Ji et al. [23]. Catalysts containing 5-10% Co showed the highest performance or lowest light-off temperature among the prepared catalysts (T_{90}=562°C). Ulla et al. [23] also prepared CoOMgO solid solutions by impregnating MgO with 3-12 wt.% cobalt and calcination at temperatures higher than 1073 K. A threshold of 9 wt.% was reported for the cobalt loading. The availability of Co^{2+} on the surface of the catalyst was the key factor in catalytic activity. Reduction of Co dispersion and blockage of Co active sites were the main causes of activity reduction at loadings higher than 9%. 20% $LaMnO_3$ perovskite was supported on MgO [25]. The supported $LaMnO_3$ catalysts showed superior activity compared to the non-supported one. Furthermore, MgO is used as a promoter for the support or active metal species in CMC. The insertion of MgO to alumina support [26] and the formation of $MgAl_2O_4$ phase increased the dispersion of PdO compared to bare Al_2O_3. It also regulated the PdO lattice and the support active metal interaction due to its relatively acidic and basic sites. Zhao et al. [27] reported that the addition of MgO to the catalyst stabilized the PdO active metal against the formation of $Pd(OH)_4$ in the presence of water and increased the catalyst activity and stability. MgO was inserted into CeO_2 as the support of Ni, Co and Cu [28]. Ni supported on Mg promoted supports showed the highest activity and stability, while pure Ni/MgO catalyst revealed the lowest activity in the CMC reaction. Mg promotion of $LaCrO_3$ catalysts and substitution of Cr/Mg increased the catalytic activity of the perovskite catalyst. The Mg substitution reduced the crystallite size and the sintering tendency of the catalyst [29]. In addition, La_2MnNiO_6-MgO mixed oxide prepared by the biphasic intergrowth method showed superior activity in the CMC process [30]. Insertion of Mg^{2+} into the perovskite's structure improved its defect concentration and reduction properties, resulting in higher activity and stability of the catalyst compared to the pure perovskite catalyst.

Fe or α-Fe_2O_3 with no support have been studied by Paresed et al. [31] and Dong et al. [32] in the CMC process. In both studies, the crystal structure of Fe_2O_3 was identified as the critical parameter in catalytic activity. The prepared Fe_2O_3 catalysts underwent structural changes and agglomeration at higher temperatures, which caused a severe decrease in catalytic activity. FeO_x or Fe_2O_3 possesses redox and oxygen vacancy properties. Redox properties activate methane molecules by engaging them in the oxidation process. The oxygen vacancies act as active sites for methane adsorption and activation. CuO_x supported on mordenite zeolite (MOR) was investigated by Wang et al., demonstrating a great catalytic activity at low temperatures due to its redox properties. The 6%CuO_x/MOR catalyst prepared at pH=7.0 achieved T_{90} at 350 °C. The catalyst showed different CuO_x species (Cu^{2+}, Cu^{1+} and Cu^0) on the surface of the catalyst, considering the pH of the preparation environment and interactions with Al^{3+} of the MOR support [33].

Considering the mentioned exceptional properties of MgO, in this research, we have prepared MgO through a precipitation process as the support of Fe active metal. Supported Fe catalysts are evaluated in this study. The catalysts were prepared by a simple impregnation technique with different loadings (10-20%). Subsequently, the addition of Cu (3-5%) as a promoter to the Fe active metal was assessed.

2. Experimental

2.1. Support and catalyst preparation

Copper nitrate [$Cu(NO_3)_2.3H_2O$, Merck, 99.9%], ferric nitrate [$Fe(NO_3)_3.9H_2O$, RANKEM, 98%], magnesium nitrate ($Mg(NO_3)_2$. $6H_2O$, Lochemie, 98.5 %) have been used as the precursors. Sodium carbonate [Na_2CO_3, LOBA Chemie, 99.9%] was used as the precipitating agent. The MgO support was prepared through the precipitation technique. An appropriate amount of magnesium nitrate was dissolved in 100 mL of distilled water, followed by precipitation using sodium carbonate. The precipitation continued until the pH reached 10. The solution was mixed for another 4 hours, followed by filtration, drying (at 80 °C) and calcination at 650 °C. The catalysts employed in the present work were prepared by

10.57647/ijc.2026.1601.03

impregnation or the simultaneous impregnation method. In the impregnation method for the synthesis of 1 gr Fe/MgO catalyst, 0.52-1.04 gr of $Fe(NO_3)_3.9H_2O$ was dissolved in 20 ml de-ionized water, while 0.8-0.9 gr MgO as support, depending on the loading of Fe, was added to the solution. The slurry was aged for 4 hr at room temperature. The samples were dried at 80˚C overnight and calcined at 550ºC for 4 hr. The promoted catalysts were synthesized using a simultaneous impregnation process. In promoted samples 0.091 or 0.15 gr Cu $(NO_3)_2.3H_2O$ were dissolved along with 0.78 gr Fe $(NO_3)_3.9H_2O$ in 20 ml distilled water., Afterwards, 0.82 or 0.8 gr MgO support was added to the solution, to obtain 15Fe-3Cu /MgO and 15Fe-5Cu/MgO catalysts. The Aging, drying and calcination were the same as those used for the Fe impregnated samples.

2.3. Catalysts characterization

The XRD patterns were recorded on an X-ray diffractometer (PAnalytical X'Pert-Pro) using a Cu-Kα monochromatized radiation source and a Ni filter on the range 2θ=20-80º. Energy dispersive X-ray spectroscopy (EDS/EDX) and SEM-EDS elemental mapping were performed by Nova NanoSEM 450 (FEI) to detect and measure the metal loadings in samples. The surface area and porosity of both the support and catalysts were assessed through N_2 adsorption-desorption test, utilizing a BELSORP Mini II device. The BET (Brunauer-Emmett-Teller) method was applied to measure the surface area; however, porosity was calculated by using the BJH method.

2.4. Catalyst testing

The tests were carried out in a fixed-bed quartz reactor (i.d. of 8 mm), with temperature ranging from 350 to 600 °C at atmospheric pressure. The temperature of the reactor was controlled by a thermocouple located in the middle of the reactor (an electrical heater is employed). Gases consisting of methane, oxygen and argon controlled by MFC were fed to the reactor. The molar ratio of oxygen to methane of 2:1 was used. Ar was also added to the feed to keep the gas hourly space velocity (GHSV) at 21000hr^{-1}. 200 mg of catalyst with a mesh of 40-60 was loaded in the reactor for all tests. Quartz fillings were used along with the catalyst for better distribution of the inserted gases. The catalysts were oxidized in situ by 20ml/min oxygen at 400 °C for 1 hour prior to the reaction. Outlet gases passed through the condenser, and the dried gas products were analyzed by a Shimadzu-8A chromatograph equipped with a thermal conductivity detector and a Carbosieve column. The accuracy of the tests was controlled by carbon balance (C_{in}-C_{out} < ε). Reaction parameters were defined according to the following equations:

$$X_{CH4}(\%) = \frac{CH_{4in} - CH_{4out}}{CH_{4in}} \times 100 \quad (2)$$

X_{CH4} represents the CH_4 conversion. $CH_{4\ in\ or\ out}$ is the molar flow rate of methane at the inlet or outlet of the reactor.

3. Results and discussion

3.1. Catalyst characterization

The XRD patterns of MgO support, Fe and Fe-Cu catalysts are presented in the Fig. 1a &b. The XRD pattern of Fig. 1a shows the formation of a pure MgO structure. According to JCPDS card No. 75-1525, peaks corresponding to MgO appear at 2θ=37.14º (111), 43.07º (200), 62.42º(220), 73.75º(311) and 78.70º(222). In XRD patterns of 15% and 20% Fe supported on MgO, in addition to diffractions related to MgO, diffractions of α-Fe_2O_3 at 2θ= 18.93º (012), 35.49º (104), 50.75º (024), 58.65º (018) and 62.37º (214) can be observed (according to JCPDS card No. 33-0664). Some of the peaks corresponding to α-Fe_2O_3 overlap with the diffractograms of MgO. There is also a strong possibility of $MgFe_2O_4$ phase or Fe-Mg solid-solution formation ($Mg_{1-x}Fe_xO$). The peaks related to $MgFe_2O_4$ appear at 2θ= 19.50º (111), 30.1º(220), 35.6º(311), 45.6º(400), 54.65º (422) and 63.05 º(440) according to JCPDS card No. 036-0398. The formation of solid solution usually begins to appear at temperatures higher than 400 ºC and increases with calcination temperature [34].

In Fig. 1b, for the 15Fe-5Cu sample, besides the diffractograms of MgO and α-Fe_2O_3 or Fe-Mg solid solution ($MgFe_2O_4$), peaks corresponding to CuO at 2θ= 35.31 º (-111), 38.37 º(111), 49.77 º (-202) were detected according to JCPDS card No. 80-0076. Althoughthe CuO might be inserted into MgO or Fe structures, this is not evident in diffractograms due to low loadings of CuO. Most CuO peaks showed an overlap with diffractograms of MgO, Fe_2O_3 or $MgFe_2O_4$.

The crystallite size was determined by X-ray diffraction using Scherrer's formula:

$$D_{XRD} = \frac{0.9\,\lambda}{\beta\,cos\theta}$$

Where D_{XRD} is the crystalline size calculated by XRD, λ is the X-ray wavelength, β is the half-width of diffraction peaks, and θ is the angle of diffraction. The crystalline size of the support and catalysts is available in Table 1.

10.57647/ijc.2026.1601.03

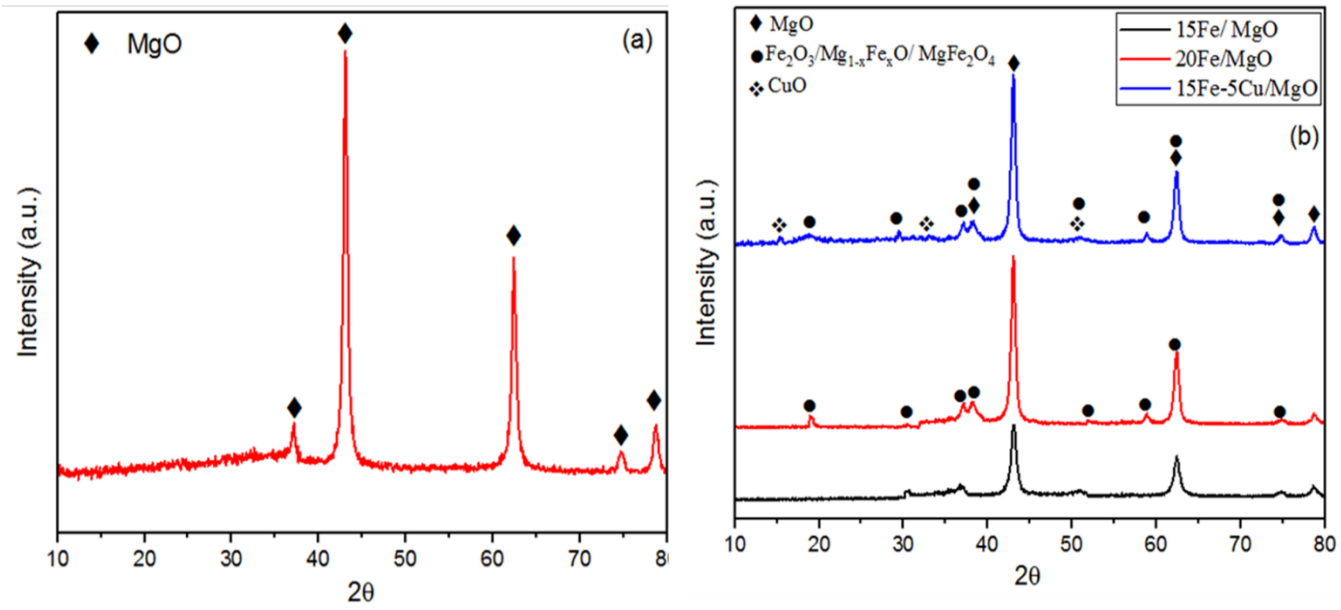

Figure 1. XRD patterns of a) MgO support, b) Fe/MgO catalysts and 15 Fe-5Cu/MgO catalyst

Table 1. Properties of MgO support and Fe or Fe-Cu catalysts supported on MgO

Sample	D_{XRD} [1](nm)	BET surface area ($m^2.g^{-1}$)	Mean pore diameter (nm)	Total pore volume ($cm^3.g^{-1}$)	Mean particle size[2] (nm)
MgO	21.91	83.51	31.90	0.6661	54.07
15 Fe/MgO	16.17	-	-	-	-
20Fe/MgO	22.95	49.70	40.22	0.4998	91.73
15Fe-5Cu/MgO	31.2	30.26	34.06	0.2577	99.5

[1] calculated using XRD diffractograms
[2] calculated from BET data.

The crystallite size of the MgO support was calculated using the (111), (200), (220), (311), and (222) planes. For the catalysts, the calculation of the average crystallite size included planes corresponding to the different phases present: specifically, the (012), (104), (110), and (024) planes for Fe_2O_3; the (220), (311), (400), and (440) planes for $MgFe_2O_4$; and the (-111), (111), (-202), and (020) planes for CuO.

The MgO support had a crystallite size of 21.91 nm. Impregnation of the support with Fe and Cu loadings higher than 10 wt.% increased the crystallite size. For example, the 15Fe-5Cu/MgO catalyst exhibited a larger crystallite size of 31.2 nm.

As shown in Table 1, the surface area of the MgO support decreased after impregnation with Fe and Cu. Impregnation of the support with 20Fe and 15Fe-5Cu reduced the BET surface area to 49.7 $m^2.g^{-1}$ and 30.26 $m^2.g^{-1}$, respectively. Although, 20 Fe and 15Fe-5Cu have the same theoretical active metal content but the sample impregnated with Cu showed more reduction in BET surface area. EDS analysis and SEM-EDS elemental mapping were used to determine the Fe and Cu loadings in the promoted and non-promoted samples (Fig. 2). The results showed Fe loadings of 17.08 wt.% and 12.18 wt.% for the 20Fe/MgO and 15Fe-5Cu/MgO samples, respectively. A Cu loading of 2.91 wt.% was detected in the 15Fe-5Cu/MgO sample. The EDS analysis revealed that the actual active metal loadings were lower than the theoretical values for both samples. The nitrogen adsorption/desorption isotherms for the MgO support, 20Fe/MgO and 15 Fe-5Cu/MgO catalysts are presented in Fig. 3a.

The isotherms exhibit type IV curves with an H3-type hysteresis loop, which is characteristic of mesoporous materials (pore diameters between 2–50 nm).

The H3 loop is indicated by a desorption branch occurring at a lower relative pressure compared to other hysteresis types; for N_2 adsorption at 77 K, this is located in the region of $P/P_0 = 0.42$ [35-36].

This type of hysteresis is typically for pores formed by flaky particles. Figure 3b shows the pore size distribution of the prepared MgO support, 20Fe/MgO and 15Fe-5Cu/MgO catalysts. The MgO support and catalysts display a bimodal (mesoporous-macroporous) pore size distribution. The average pore diameters for the MgO support, 20Fe/MgO and 15Fe-5Cu/MgO catalyst are 31.9 nm, 40.2 nm and 34.06 nm, respectively. The support exhibited a narrower pore size distribution compared to the catalysts; however, the reverse was observed for the pore volume.

10.57647/ijc.2026.1601.03

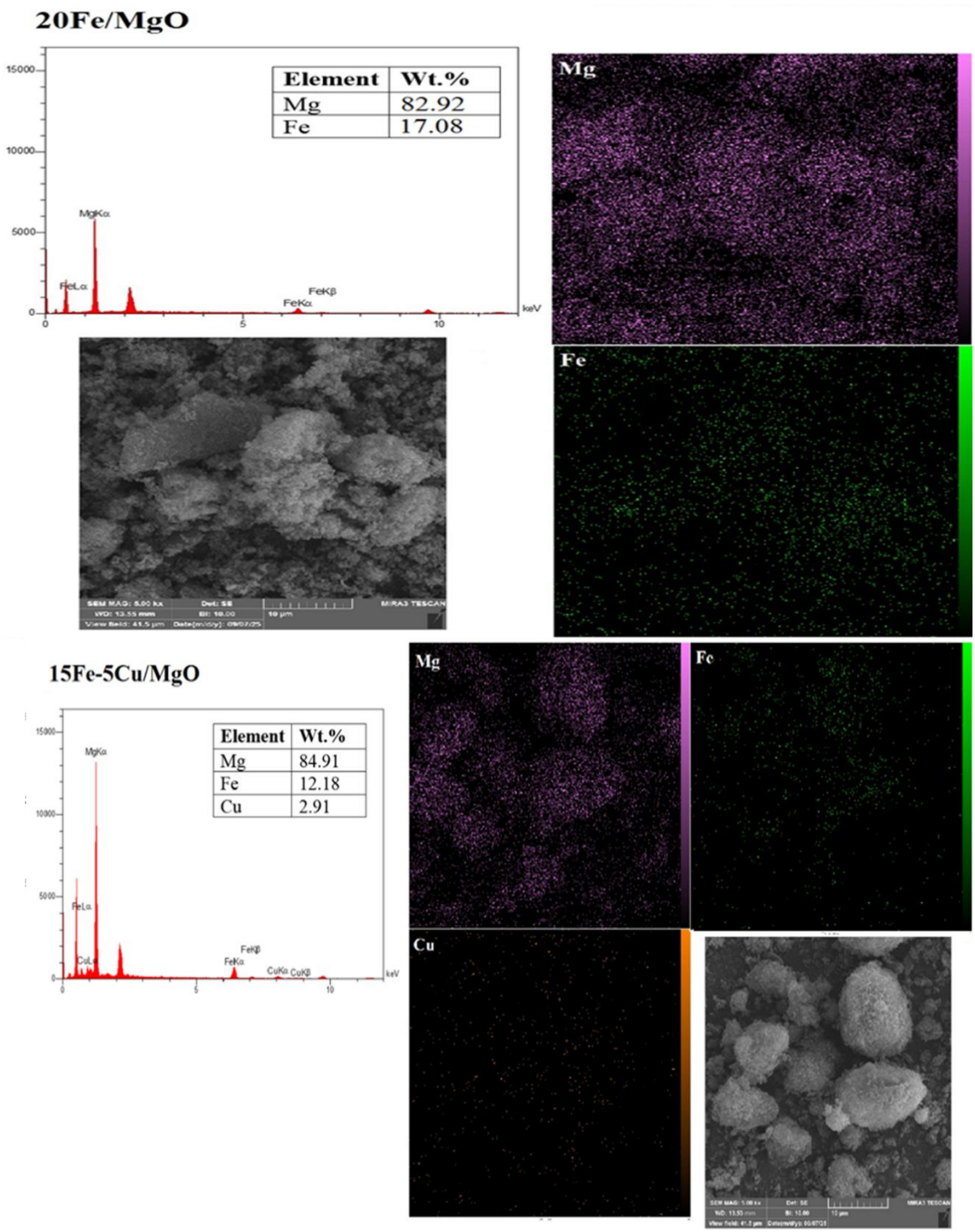

Figure 2. EDS spectrum and SEM-EDS elemental mapping of 20Fe/MgO and 15Fe-5Cu/MgO catalysts

3.2. Catalytic activity

3.2.1. *Fe/MgO catalysts*

The conversion of methane versus temperature is presented in Fig. 4. Since the methane combustion reaction is exothermic, the increase in temperature elevated the methane conversion.

Different Fe loadings, ranging from 10 to 20 wt%, were evaluated (xFe/MgO; x=10, 15, and 20%). An increase in Fe loading enhanced the catalytic activity, with the 20% Fe and 10% Fe catalysts demonstrating the highest and lowest catalytic performance, respectively, among the synthesized catalysts. Several mechanisms are proposed for methane combustion, including the Langmuir-Hinshelwood (LH) mechanism, the Eley-Rideal mechanism, and the Mars-van Krevelen mechanism. The LH and Eley-Rideal mechanisms are the most plausible for Fe/MgO catalysts, as the support is a metal oxide with no oxygen vacancies. Key steps in the catalytic methane combustion according to the LH mechanism are [37]:

1. Adsorption of reactants, methane and oxygen stick to active sites on the catalyst surface; 2. Activation and dissociation, methane and oxygen bonds are broken and dissociated into reactive species; 3. Surface reactions, Intermediate species react to form CO_2 and H_2O; 4. Products desorption: the products are desorbed from the active sites, freeing active sites for further reactions. As stated in the reaction mechanism, the higher availability of active sites with increased Fe loading promoted greater adsorption of methane and oxygen, which led to higher methane conversions.

A higher loading of FeOx or Fe_2O_3 on the MgO surface can also enhance redox properties and generate oxygen vacancies. These properties allow more methane molecules to be activated and participate in the oxidation reaction [38].

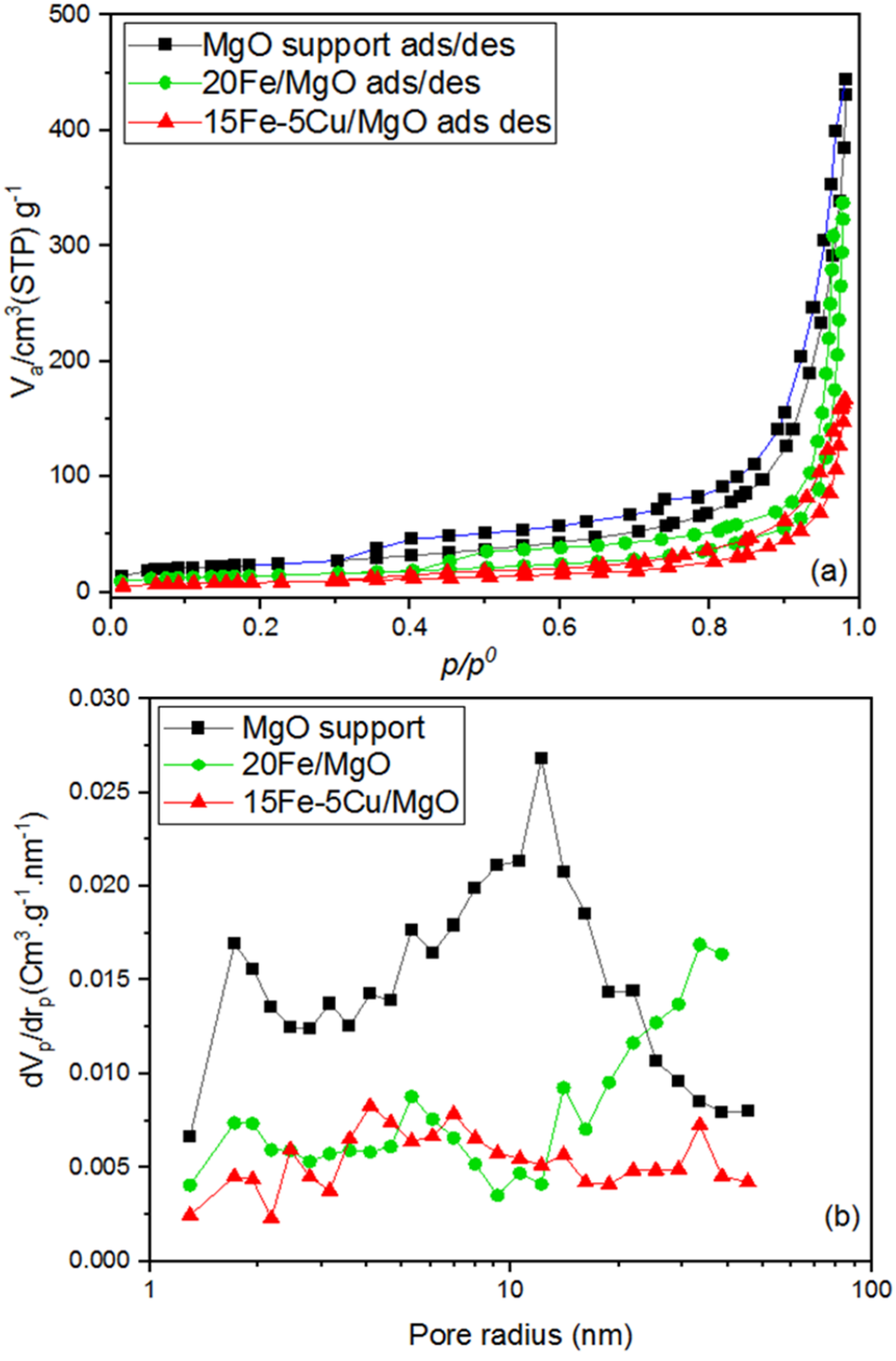

Figure 3. (a) Adsorption/ desorption isotherms and (b) pore size distribution of MgO support, 20 Fe/MgO and 15Fe-5Cu/MgO catalysts

10.57647/ijc.2026.1601.03

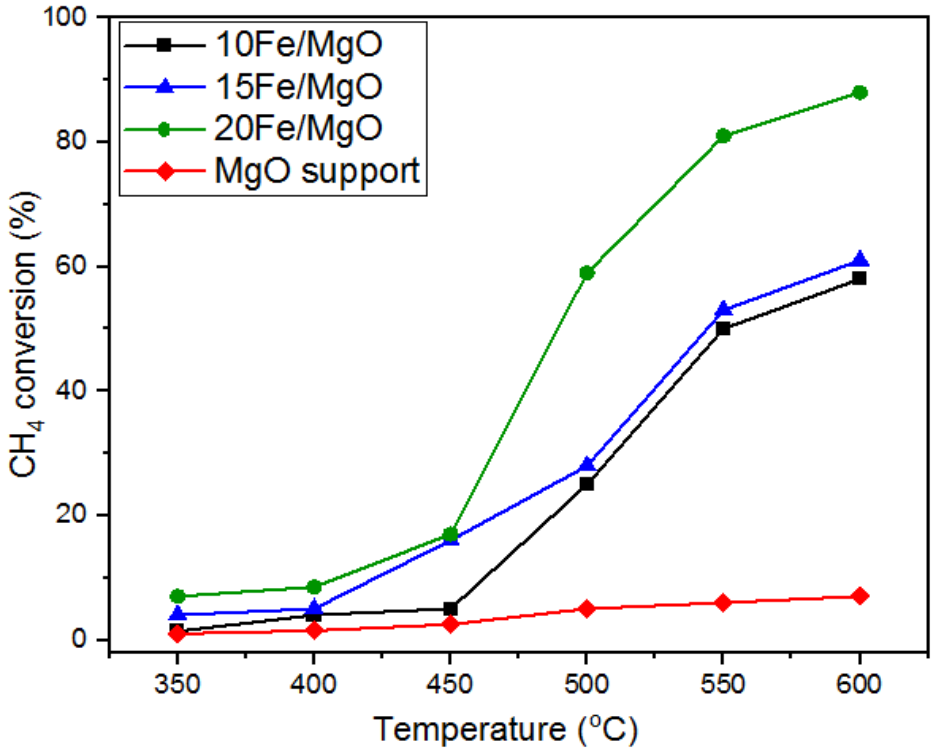

Figure 4. CH_4 conversion of Fe/MgO catalysts at different temperatures, O_2:CH_4=2, GHSV=21000h^{-1}

As a result of magnesium oxide's high surface area (83.51 $m^2 \cdot g^{-1}$), increasing the Fe loading to 20% did not significantly reduce the number of total active sites or the metal dispersion. After impregnation of MgO with 20% Fe, the catalyst still showed a high surface area. The 10 wt% and 20 wt% Fe catalysts achieved methane conversions of 60% and 89% at 600 °C, respectively. The light-off temperatures, T_{10} and T_{50}, for the 20% Fe catalyst were 412 °C and 463 °C, respectively. On the other hand, in studies of active iron species in Fe/MgO catalysts, Boudart et al. [39] revealed that in the reduced state, Fe^{2+} cations and Fe^0 species were present, while in the oxidized state, Fe^{3+} cations were dispersed over/within the MgO matrix and in the form of $MgFe_2O_4$. As discussed in the characterization section, the XRD patterns (Fig. 1b) indicate a high likelihood of partial solid solution formation in the Fe/MgO catalysts. The high activity of Fe/MgO catalysts at higher Fe loadings can be attributed to the greater availability of Fe^{3+} cations and their interaction with the O^{2-} sites of the basic support [40]. Further investigations were performed on the 15% Fe catalyst. In this research, we aimed to improve the catalytic activity of 15Fe by adding Cu as a promoter. The total active metal loading was not increased beyond 20% to prevent the agglomeration of active metal species on the catalyst surface and to limit the intensification of $Mg_{1-x}Fe_xO$ solid solution (or $MgFe_2O_4$) formation.

3.2.2. *Fe-Cu/MgO catalysts*

The CH_4 conversion versus temperature of 15Fe-yCu/MgO (y=3 and 5%) is exhibited in Fig. 5. Similarly, as the temperature rose, CH4 conversions increased, but to a much lesser extent compared to the unpromoted catalyst. The addition of Cu, especially 5 wt.%, slightly improved the catalytic activity of 15Fe at temperatures below 400 °C by enhancing the redox properties of the catalyst [33]. However, at higher temperatures, it had an undesirable effect on the catalytic performance. The lower activity of Cu-promoted catalysts at temperatures higher than 400 °C can be related to a decrease in Fe metal active sites or limited access of the reactants to the active sites. As Cu was introduced by a simultaneous impregnation method in this research, some of the available active sites are probably blocked by Cu metal, which is easily converted to CuO_x in the presence of oxygen. It is well known that CuO_x species are less active for the methane combustion at high temperatures due to agglomeration and a decrease in redox properties. The Cu promoted catalyst (15Fe-5Cu) showed lower BET surafce area compared to 20 Fe catalyst, which confirmed agglomeration of catalyst with introduction of Cu to catalyst. In other words, the addition of copper to Fe leads to a decrease in catalytic activity by reducing the amount of exposed active atoms available to reactant molecules [41-43]. Reyes et al. reported as well that the addition of Cu promoter (0.3-1.2wt.%) to Pd/SiO_2 catalyst decreased the catalytic activity or increased the light-off temperatures. They attributed this phenomenon to variation in the nature of the active sites caused by the Cu-Pd alloying and not to partial coverage of Pd particles, as it was determined by XPS analysis [42]. Similar findings were reported for $Pt\text{-}Cu/Al_2O_3$ catalysts by Papa et. al [43]. Pt atoms were decorated by Cu oxide species. The

10.57647/ijc.2026.1601.03

alloyed Pt particles with copper were less active than the non-alloyed particles. Shafaei et al. prepared Co-Fe, Cu-Fe, and Ni-Fe mixed oxides or alloys and evaluated them in the methane combustion process. Among the prepared mixed oxides, Cu-Fe or CuFe2O4 showed the lowest activity [44]. Furthermore, the activity of Cu as a promoter or active metal depends strongly on the nature of the support. CuO is less active on supports like Al_2O_3 and SiO_2 and shows greater activity on ZrO_2 [45] or CeO_2 [46]. ZrO_2 or CeO_2 with their vacancies interact with Cu, in this way highly dispersed and active Cu species were observed. Cu was supported on MgO, Al_2O_3 and Mg_xAl_yO by Popescu et al. [47]. Lowest acitvity was observed for Cu/MgO catalyst or the purely basic support. The support with both basic and acidic sites (CuMgAl(1)O) showed the highest activity. The adsorption of reactants and desorption of products are affected by both Lewis acidic (metal cations) and basic sites (lattice oxygen anions) [48]. Considering the obtained results in this research and reports of other researchers, the decline in catalytic activity after introudction of Cu to Fe/MgO catalysts is reasonable.

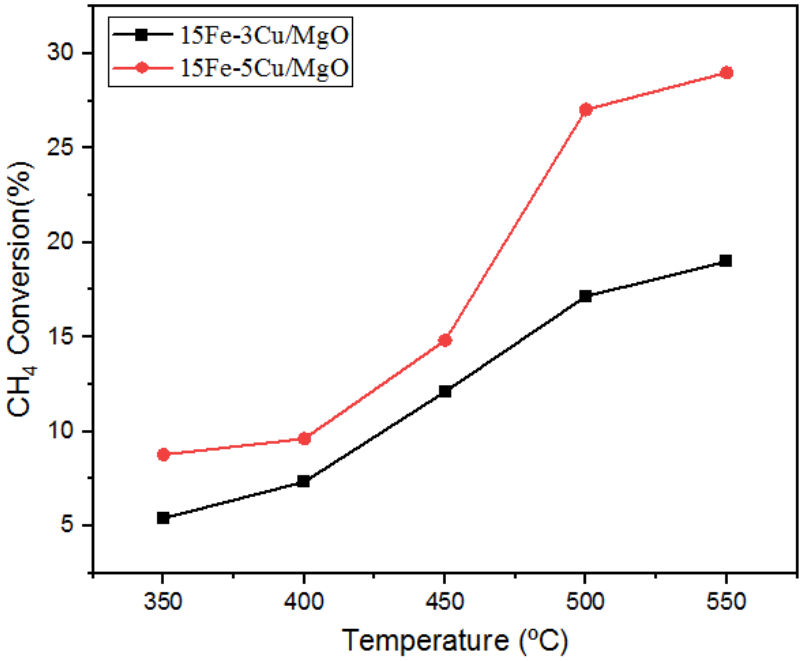

Figure 5. CH_4 conversion of Fe-Cu/MgO catalysts at different temperatures, O_2:CH_4=2, GHSV=21000h^{-1}

Table 2. Comparison of the catalyst presented in this work with similar supported catalysts

No.	Catalyst	CH_4 feed concentration (%)	GHSV mL/g_{cat}.h	T_{50}(°C)	T_{90}(°C)	Ref.
1	Fe/MgO	2	480000	> 675	-	[49]
2	Co/MgO	2	480000	>622	-	[23]
3	Co/MgO	1	40000	500	550	[22]
4	CuAlO	1	20000	530	564	[47]
	CuMgAl(1)O			525	554	
	CuO/MgO			580	625	
5	3%Cu/Al_2O_3	1.4	30000	475	535	[45]
	6%Cu/ZrO_2			480	540	
	1.3%Cu/SiO_2			660	-	
6	CuO_x/MOR (zeolite)	0.2	5000	300	350	[33]
7	Co/Al_2O_3	1	60000	491	560	[50]
	Co-Cu/Al_2O_3			475	589	
8	Fe_2O_3/Al_2O_3Foam	<5	-	-	>600	[51]
9	Fe/Al_2O_3	-	7200	550	632	[52]
	Fe/Al_2O_3-SiO_2			702	-	
10	Fe/TiO_2	1	6000	502	610	[53]
11	20Fe/MgO	10	21000	463	~600	present work

10.57647/ijc.2026.1601.03

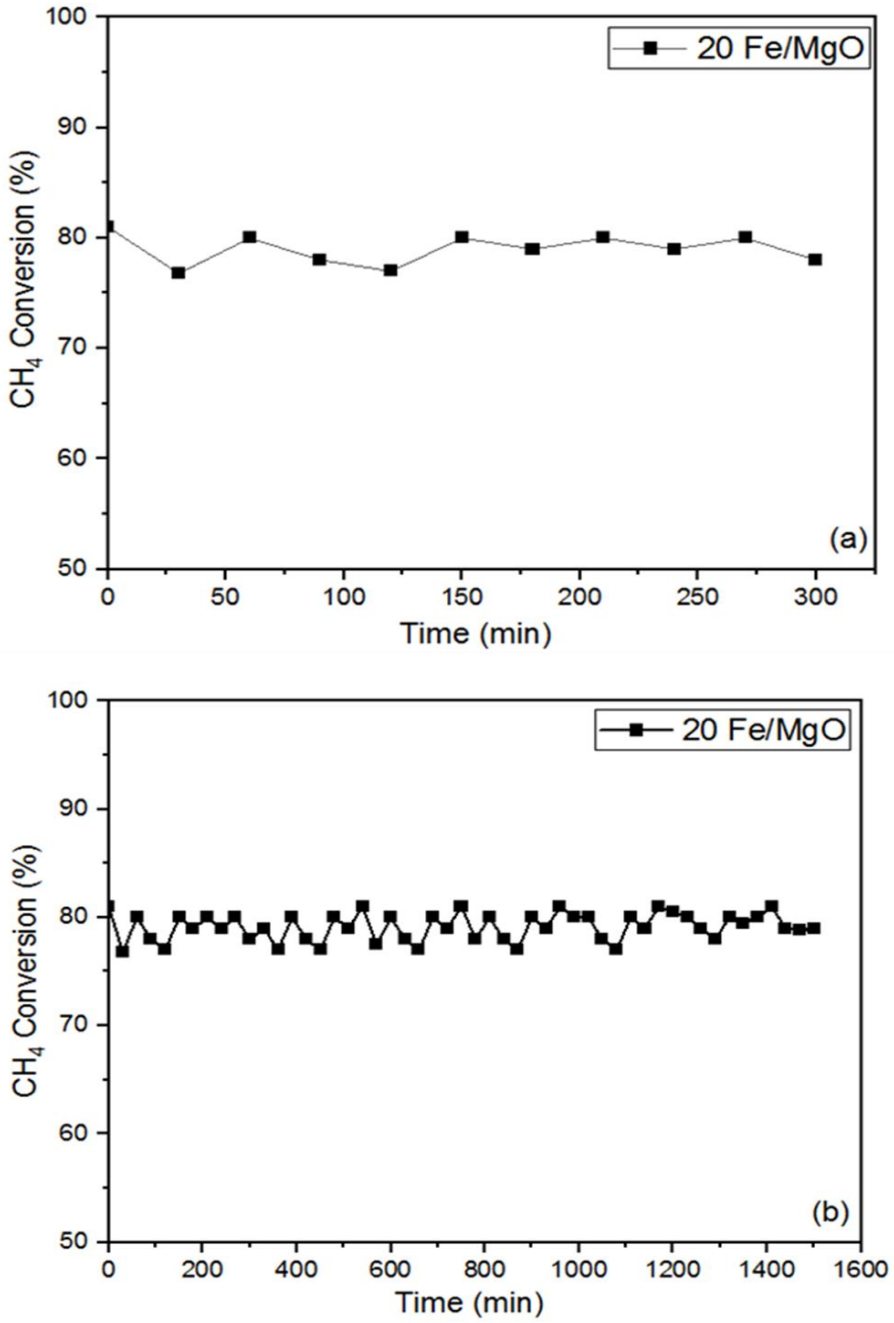

Figure 6. CH_4 conversion of 20Fe/MgO catalyst at 550°C during a) 5 h & b) 25 h on stream, O_2:CH_4=2, GHSV=21000h^{-1}

A comparison between the best catalyst from this work and those reported in similar studies on metal-supported catalysts for methane combustion is presented in Table 2. As shown in Table 2, the 20Fe/MgO catalyst described in this research exhibits excellent activity compared to other Fe-based catalysts. However, recently evaluated Cu catalysts supported on Al_2O_3 or transition metal oxides displayed higher activity, with lower T_{50} and T_{90} values reported. Because the 20Fe/MgO catalyst showed the highest activity among the prepared samples, its stability was evaluated.

3.3.3. *Stability of 20Fe/MgO catalyst*

The short- and long-term stability of the optimum catalyst (20Fe/MgO) during 5 h and 25 h on stream at 550 °C are illustrated in Fig. 6 a & b. The catalyst showed no obvious decrease in catalytic activity during 5 or 25 h on stream, with CH_4 conversions > 80%.

XRD analysis was performed on the 20Fe/MgO catalyst after 5 h on stream (Fig. 7) to examine its structural stability.

The diffractograms show that the peaks corresponding to the $Mg_{1-x}Fe_xO$ solid solution and/or Fe_2O_3 became more intense.

This indicates that exposure to the oxidizing environment for 5 hours promoted the transformation of the major crystalline phase from MgO to the $Mg_{1-x}Fe_xO$ solid solution. However, this phase change had an insignificant effect on the catalytic activity. The spent catalyst had a crystallite size of 29.1 nm after being on stream for 5 h. at 550 °C.

10.57647/ijc.2026.1601.03

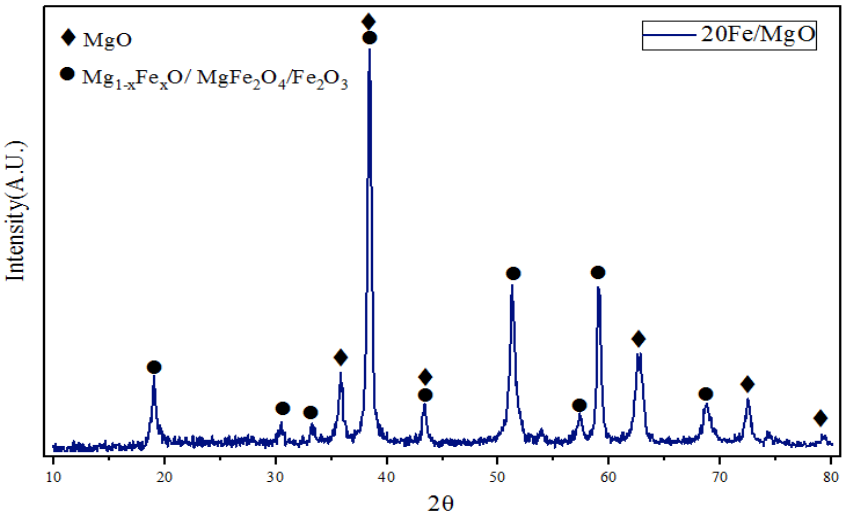

Figure 7. XRD pattern of 20Fe/MgO after 5 h on stream at 550 ºC, O_2/CH_4=2, GHSV=21000h^{-1}

4. Conclusions

Catalytic combustion of methane (CMC) oxidizes methane at temperatures significantly lower than traditional thermal combustion. However, finding catalysts that are stable and operate at low temperatures remains a key challenge. In this study, Fe/MgO-based catalysts demonstrated high activity for the methane combustion reaction. Among them, the 20Fe/MgO catalyst, which had the highest iron loading and a specific surface area of 49.70 $m^2 \cdot g^{-1}$, exhibited the best catalytic performance.

In contrast, the addition of Cu as a promoter to the 15Fe/MgO catalyst reduced its catalytic activity, particularly at temperatures above 400 °C. This decrease in activity is attributed to the blocking of active sites by Cu species or the alteration of their nature, and the agglomeration of particles caused by the insertion of Cu. The 20Fe/MgO catalyst displayed excellent stability over a 25-hour test period.

Conflict of interest
The authors declare that they have no known competing financial interests or personal relationships that could have appeared to influence the work reported in this paper.

Data availability statement: All the data relevant to this research project have been included in the manuscript.

Funding Declaration
The authors declare that no funding was received during the preparation of this manuscript.

References

[1] M. Filonchyk, M. P. Peterson, L. Zhang, V. Hurynovich, Y. He, Sci. Total Environ. **935** (2024). 173359. http//: doi.org/10.1016/j.scitotenv.2024.173359

[2] X. Zhang, X. Zhang, L. Ren, M. Han, N. Feng, H. Wan, G. Guan, Fuel **379** (2025) 133090. http//: doi.org/10.1016/j.fuel.2024.133090

[3] T. V. Choudhary, S. Banerjee, V. R. Choudhary, Appl. Catal., A **234** (2002) 1-23. http//: doi.org/10.1016/S0926-860X(02)00231-4

[4] X. Feng, L. Jiang, D. Li, S. Tian, X. Zhu, H. Wang, K.Li, J. Energy Chem. **75** (2022) 173-215. http//: doi.org/10.1016/j.jechem.2022.08.001

[5] J. Chen, H. Arandiyan, X. Gao, J. Li, Catal. Surv. Asia **19** (2015) 140-71. http//: doi.org/10.1016/j.rser.2019.109589

[6] Z. Tang, T. Zhang, D. Luo, Y. Wang, Z. Hu, R. T. Yang, ACS Catal. **12** (2022) 13457-74. http//: doi.org/10.1021/acscatal.2c01012.

[7] R. Abbasi, L. Wu, S. E. Wanke, R. E. Hayes, Chem. Eng. Res. Des. **90** (2012) 1930-1942. http//: doi.org/10.1016/j.cherd.2012.03.003

[8] R. S. Kumar, J. P. Mmbaga, N. Semagina, R. E. Hayes, Catal. **14** (2024) 319-44. http//: doi.org/10.3390/catal14050319

[9] R. Burch, P. K. Loader, Appl. Catal., B **5** (1994) 149-64. http//: doi.org/10.1016/0926-3373(94)00037-9

[10] C. Zhang, X. Chen, X. Zhang, S. Chen, S. Gao, D. Yu, Z. Zhao, J. Mater. Chem. **13** (2025) 8024-34. http//: doi.org//10.1039/d5ta00639b

[11] K. Narui, K. Furuta, H. Yata, A. Nishida, Y. Kohtoku, T. Matsuzaki, Catal. Today. **45** (1998) 173-78. http//: doi.org/10.1016/S0920-5861(98)00274-0

[12] D. Gao, C. Zhang, S. Wang, Z. Yuan, S. Wang, Catal. Commun. **9** (2008) 2583-87. http//: doi.org/0.1016/j.catcom.2008.07.014.

[13] T. S. Cam, T. A. Vishnevskaia, V. I. Popkov, Rev. Adv. Mater. Sci. **59** (2020) 131-43. http//: doi.org/10.1515/rams-2020-0002

[14] X. Wei, J. Kang, L. Gan, W. Wang, L. Yang, D. Wang, J. Qi, Nanomaterials **13** (2023) 1917-49. http//: doi.org/10.3390/nano13131917

[15] A. Setiawan, E. M. Kennedy, B. Z. Dlugogorski, A. A. Adesina, M. Stockenhuber, Catal. Today **258** (2015) 276-283. http//: doi.org/10.1016/j.cattod.2014.11.031

[16] E. Akbari, S. M. Alavi, M. Rezaei, A. Larimi, Int. J. Hydrogen Energy **47** (2022)13004-21. http//: doi.org/10.1016/j.ijhydene.2022.02.070

[17] M. M. Fiuk, A. Adamski, Catal. Today **257** (2015) 131-35. http//: doi.org/10.1016/j.cattod.2015.01.029

[18] S. Cimino, S. Colonna, S. De Rossi, M. Faticanti, L. Lisi, I. Pettiti, P. Porta, J. Catal. **205** (2002) 309-17. http//: doi.org/10.1006/jcat.2001.3441

[19] S. Wang, Y. Zhang, S. Zhao, Y. Zhang, Y. Wang, Y. Zhang, S. Qiao, Mol. Catal. **531** (2022) 112685. http//: doi.org/10.1016/j.mcat.2022.112685.

[20] J. Xu, Z. Tian, Y. Xu, Z. Xu, L. Lin, Stud. Surf. Sci. Catal. **147** (2004) 481-486. http//:doi.org/10.1016/S0167-2991(04)80098-3

[21] S. Trivedi, R. Prasad, J. Environ. Chem. Eng. **4** (2016) 1017-28. http//:doi.org/ 10.1016/j.jece.2016.01.002

[22] S. Jayasree, A. Manikandan, A. M. Mohideen, C. Barathiraja, S. A. Antony, Adv. Sci., Eng. Med. **7**(8) (2015) 672-82. http//: doi.org/10.1166/asem.2015.1750

[23] S. F. Ji, T. C. Xiao, H. T. Wang, E. Flahaut, K. S.Coleman, M. L. Green, Catal. Lett. **75** (2001) 65-71. http//: doi.org/ 10.1023/A:1016711207912

[24] M. A. Ulla, R. Spretz, E. Lombardo, W. Daniell, H. Knözinger, Appl. Catal., B **29** (2001) 217-29. http//: doi.org/10.1016/S0926-3373(00)00204-6

[25] E. E. Svensson, S. Nassos, M. Boutonnet, S. G. Järås, Catal. Today **117** (2006) 484-90. http//: doi.org/10.1016/j.cattod.2006.06.014

[26] J. Li, Y. Zhang, W. Shan, H. He, Fuel **340** (2023) 127493. http//: doi.org/10.1016/j.fuel.2023.127493

[27] G. Zhao, X. Pan, Z. Zhang, Y. Liu, Y. Lu, J. Catal. **384** (2020) 122-35. http//: doi.org/10.1016/j.jcat.2020.01.013

[28] Y. Li, Y. Guo, B. Xue, Fuel Process. Technol. **90** (2009) 652-56. http//: doi.org/10.1016/j.fuproc.2008.12.002

[29] G. Saracco, G. Scibilia, A. Iannibello, G. Baldi, Appl. Catal., B **8** (1996) 229-44. http//: doi.org/10.1016/0926-3373(95)00084-4

[30] R. Ding, C. Li, L. Wang, R. Hu, Appl. Catal., A **464** (2013)261-68. http//: doi.org/10.1016/j.apcata.2013.05.041

[31] J. R. Paredes, S. Ordóñez, A. Vega, F. V. Dıez, Appl. Catal., B **47** (2004) 37–45. http//:doi.org/10.1016/s0926-3373(03)00325-4

[32] B. Dong, H. Zhang, A. Kong, Y. Kong, F. Yang, Y. Shan, Eur. J. Inorg. Chem. **28** (2014)4779–87. http//:doi.org/10.1002/ejic.201402152

[33] Y. Wang, Y. Wang, Z. Liu, Y. Li, L. Yao, S. Shao, X. Fan, T. Ming, X. Lu, L. Mu, W. Li, Appl. Surf. Sci. **682** (2025) 161691. http//:doi.org/10.1016/j.apsusc.2024.161691

[34] X. Ge, M. Li, J. Shen, J. Solid State Chem. **16** (2001)38-44. http//:doi.org/10.1006/jssc.2001.9264

[35] K. S. Sing, R. T. Williams, Adsorpt. Sci. Technol. **22** (2004)773-82. http//:doi.org/10.1260/0263617053499032

[36] P. I. Ravikovitch, A. V. Neimark, Colloids Surf., A **187** (2001) 11-21. http//:doi.org/10.1016/s0927-7757(01)00614-8

[37] L. He, Y. Fan, J. Bellettre, J. Yue, L. Luo, Renewable Sustainable Energy Rev. **119** (2020) 109589. http//:doi.org/ 10.1016/j.rser.2019.109589

[38] Q. Zhang, Y. Li, D. An, Y. Wang, Appl. Catal., A **356** (2009) 103-111. http//:doi.org/ 10.1016/j.apcata.2008.12.031

[39] M. Boudart, A. Delbouille, J. A. Dumesic, S. Khammouma, H. Topsøe, J. Catal. **37**(3) (1975) 486-502. http//:doi.org/10.1016/0021-9517(75)90184-0

[40] J. A. Dumesic, H. Topsøe, S. Khammouma, M. Boudart, J. Catal. **37** (1975) 503-12. http//:doi.org/10.1016/0021-9517(75)90185-2

[41] H. Geng, Z. Yang, L. Zhang, J. Ran, Y. Yan, M. Guo, Int. J. Hydrogen Energy **41** (2016) 18282-90. http//:doi.org/ 10.1016/j.ijhydene.2016.08.134

[42] L. F. Yang, C. K. Shi, X. E. He, J. X. Cai, Appl. Catal., B **38** (2002) 117-25. http//:doi.org/10.1016/s0926-3373(02)00034-6

[43] F. Papa, C. Negrila, G. Dobrescu, A. Miyazaki, I. Balint, J. Nat. Gas Chem. **20** (2011) 537-42. http//:doi.org/10.1016/s1003-9953(10)60221-6

[44] A. Shafaei, and A. Irankhah, Mol. Catal. **538** (2023) 112989. http//:doi.org/ 10.1016/j.mcat.2023.112989

[45] G. Águila, F. Gracia, J. Cortés, P. Araya, Appl. Catal., B **77** (2008) 325-38. http//:doi.org/ 10.1016/j.apcatb.2007.08.002

[46] W. Yang, D. Li, D. Xu, X. Wang, J. Nat. Gas Chem. **18** (2009) 458-66. http//:doi.org/10.1016/s1003-9953(08)60141-3

[47] I. Popescu, N. Tanchoux, D.Tichit, I. C. Marcu, Appl. Catal., A **538** (2017) 81-90. http//:doi.org/ 10.1016/j.apcata.2017.03.012

[48] F.J.A. Al-Doghachi, Bull. Chem. React. Eng. Catal. **13** (2018) 295-310. http//:doi.org/10.9767/bcrec.13.2.1656.295-310

[49] R. Spretz, S. G. Marchetti, M. A. Ulla, E. A. Lombardo, J. Catal. **194** (2000) 167-174. http//:doi.org/10.1006/jcat.2000.2921

[50] J. Cheng, J. Yu, X. Wang, L. Li, J. Li, Z., Hao, Energy Fuels, **22** (2008)2131-2137. http//:doi.org/10.1021/ef8000168

[51] Y. Cao, F. Liu, C. Song, L. Yang, C. Zhai, Chem. Eng. J. **480** (2024) 148285. http//:doi.org/ 10.1016/j.cej.2023.148285

[52] S. Tanaka, K. Nakagawa, E. Kanezaki, M. Katoh, K.I. Murai, T. Moriga, I. Nakabayashi, S. Sugiyama, Y. Kidoguchi, K. Miwa, J. Jpn. Petrol. Inst. **48** (2005) 223-8. http//:doi.org/10.1627/jpi.48.223

[53] G. Pecchi, P. Reyes, T. Lopez, R. Gomez, A. Moreno, J.L. Fierro, A. Martínez-Arias, J. Sol-Gel Sci. Technol. **27**(2003)205-14. http//:doi.org/10.1023/a:1023758819596

Appendix

Symbol/Abbreviation	Description
BET	Brunauer-Emmett-Teller surface area
D_{XRD}	Crystalline size calculated by XRD
GC	Gas Chromatograph
GHSV	Gas Hourly Space Velocity
λ	X-ray wavelength
β	full width at half maximum, a diffractogram
MFC	Mass Flow Controller
XRD	X-Ray Diffraction
T_{10}	Temperature at which 10% of CH_4 is converted (light-off temperature)
T_{50}	Temperature at which 50% of CH_4 is converted (light-off temperature)
X_{CH4}	Methane conversion

10.57647/ijc.2026.1601.03